Anisotropy Creases Delineate White Matter Structure in Diffusion Tensor MRI

Gordon Kindlmann[1], Xavier Tricoche[2], and Carl-Fredrik Westin[1]

[1] Laboratory of Mathematics in Imaging, Department of Radiology, Harvard Medical School, USA
gk@bwh.harvard.edu
[2] Scientific Computing and Imaging Institute, University of Utah, USA

Abstract. Current methods for extracting models of white matter architecture from diffusion tensor MRI are generally based on fiber tractography. For some purposes a compelling alternative may be found in analyzing the first and second derivatives of diffusion anisotropy. *Anisotropy creases* are ridges and valleys of locally extremal anisotropy, where the gradient of anisotropy is orthogonal to one or more eigenvectors of its Hessian. We propose that anisotropy creases provide a basis for extracting a skeleton of white matter pathways, in that ridges of anisotropy coincide with interiors of fiber tracts, and valleys of anisotropy coincide with the interfaces between adjacent but distinctly oriented tracts. We describe a crease extraction algorithm that generates high-quality polygonal models of crease surfaces, then demonstrate the method on a measured diffusion tensor dataset, and visualize the result in combination with tractography to confirm its anatomic relevance.

1 Introduction

Diffusion tensor magnetic resonance imaging (DTI) is a popular means of assessing white matter in the central nervous system. Coherent organization of axons leads to diffusion anisotropy, and insofar as a tensor model accurately represents the form and direction of anisotropy, DTI can detect white matter architecture [1]. Fiber tractography has become the dominant method of DTI analysis, wherein the course of axons in fiber tracts is modeled by computing paths along the direction of greatest diffusivity (the diffusion tensor principal eigenvector), allowing connectivity between different brain regions to be mapped and quantified [2,3]. Clustering collects individual tracts into coherent structures that can model the shape and direction of fiber pathways [4]. Other white matter analysis methods do not use connectivity information from tractography, e.g. region-of-interest studies of fractional anisotropy (FA) [5,6].

We introduce *anisotropy creases* as a technique for extracting a skeleton of white matter directly from the intrinsic structure of FA. Scalar image processing defines *creases* as features at which the gradient is orthogonal to one or more eigenvectors of the Hessian [7]. Given the ubiquity of FA as a quantitative variable in the diffusion tensor literature, we have started by detecting creases

in FA. We propose that the ridge surfaces and ridge lines of FA coincide with the interiors of white matter fiber tracts, and that valley surfaces of anisotropy delineate the interfaces between fiber tracts that are adjacent but orthogonally oriented (such as between the corpus callosum and the cingulum bundles).

Anisotropy creases may have utility in a variety of contexts. Explicitly modeling the interfaces between adjacent but orthogonal fiber tracts may helpfully constrain non-rigid registration of tensor fields for group studies, as slight misregistration of these configurations could lead to comparison of tensor values within entirely separate pathways. The ability to extract white matter skeletons directly from tensor invariants, without the algorithmic complexity or parameter tuning of fiber tracking and clustering, could increase sensitivity in shape analysis studies. Finally, major crease features could play a role analogous to that of the cortical surface in functional imaging, namely a reference manifold onto which variables of interest are projected and analyzed [8].

2   Related Work

Creases have been an object of study for many years in different disciplines. In the context of geomorphology, de Saint-Venant [9] defines creases as the loci where the slope is minimal along the isocontours of the relief, which Haralick later reformulates in terms of the Hessian of the height function [10]. Maxwell gives a topological and global definition of ridges and valleys as watersheds and watercourses: slope lines that connect saddle points to local maxima or minima [11]. Others study creases in terms of differential geometry [12]. Eberly *et al.* motivate the idea that creases should be defined locally and be invariant with respect to a variety of transforms (rigid transforms, uniform scaling, and monotonic mappings of intensity) [7]. They also generalize the height-based definition of de Saint-Venant to d-dimensional manifolds embedded in n-dimensional image space, and observe that this definition produces good results for a medical imaging problem [7]. Other previous work focuses on extracting polygonal models of crease geometry; this is reviewed in Section 3.3.

A separate line of previous work studies feature detection in DTI by means other than tractography. Pajevic *et al.* use B-splines to generate continuous tensor fields that are differentiated to highlight anisotropy boundaries [13]. O'Donnell *et al.* use structure tensors to detect general boundaries in tensor values [14]. In both cases, results are visually evaluated by confirming a high edge strength near structural boundaries, but the techniques do not analyze the familiar FA measure, nor is the feature geometry explicitly extracted. Recent work by Smith *et al.* is most similar to our approach in that they perform voxel-based morphometry with a white matter skeleton calculated from ridges in a mean FA map (though "ridges" are not mentioned per se) [8]. By using an established mathematical definition of crease features, our technique extracts true codimension-one crease surfaces from continuous tensor fields of individual DTI scans, rather than a voxel-based ridge mask from the inherently smooth mean FA image from a set of registered scans.

3   Methods

3.1   Convolution and Differentiation

We start with a first-principles approach to measuring derivatives of FA in a tensor field. We use separable convolution between C^2 cubic splines and the tensor coefficient discrete samples to reconstruct a smooth tensor field [15,13]. By linearity, analytic derivatives of the reconstructed field are measured by convolving the sampled data with derivatives of the reconstruction kernel [16]. FA can be defined in terms of principal invariants J_i, which can in turn be expressed in terms of the tensor coefficients [5]. Differentiating these relations produces formulae for the gradient of FA in terms of the gradients of tensor coefficients:

$$\text{FA} = \sqrt{\frac{J_4 - J_2}{J_4}} \; ; \; \begin{array}{l} J_2 = D_{xx}D_{yy} + D_{xx}D_{zz} + D_{yy}D_{zz} - D_{xy}^2 - D_{xz}^2 - D_{yz}^2 \\ J_4 = D_{xx}^2 + D_{yy}^2 + D_{zz}^2 + 2D_{xy}^2 + 2D_{xz}^2 + 2D_{yz}^2 \end{array} \tag{1}$$

$$\nabla\text{FA} = \frac{J_2 \nabla J_4 - J_4 \nabla J_2}{2 J_4^2 \sqrt{1 - \frac{J_2}{J_4}}} \; ; \; \begin{array}{l} \nabla J_2 = \begin{array}{l}(D_{yy}+D_{zz})\nabla D_{xx} + (D_{xx}+D_{zz})\nabla D_{yy} + (D_{xx}+D_{yy})\nabla D_{zz} \\ \quad - 2D_{xy}\nabla D_{xy} - 2D_{xz}\nabla D_{xz} - 2D_{yz}\nabla D_{yz}\end{array} \\ \nabla J_4 = \begin{array}{l} 2D_{xx}\nabla D_{xx} + 2D_{yy}\nabla D_{yy} + 2D_{zz}\nabla D_{zz} \\ \quad + 4D_{xy}\nabla D_{xy} + 4D_{xz}\nabla D_{xz} + 4D_{yz}\nabla D_{yz} \end{array} \end{array} \tag{2}$$

Formulae for the second derivative (the Hessian) are longer but straight-forward to derive. Because FA is a non-linear function of the tensor, pre-computing FA on a discrete grid and then differentiating is *not* equivalent to this approach.

3.2   Crease Feature Definition

Crease features are defined in terms of the gradient $\mathbf{g} = \nabla f$ and Hessian $\mathbf{H}$ of a scalar field f [7]. Section 3.1 described how to measure the derivatives of FA at any point in a tensor field. Let $\lambda_1 \geq \lambda_2 \geq \lambda_3$ be the eigenvalues of $\mathbf{H}$, and $\{\mathbf{e}_1, \mathbf{e}_2, \mathbf{e}_3\}$ be the corresponding eigenvectors. Ridges and valleys are defined by:

	Surface	Line
Ridge	$\mathbf{g} \cdot \mathbf{e}_3 = 0, \; \lambda_3 < 0$	$\mathbf{g} \cdot \mathbf{e}_2 = \mathbf{g} \cdot \mathbf{e}_3 = 0, \; \lambda_3, \lambda_2 < 0$
Valley	$\mathbf{g} \cdot \mathbf{e}_1 = 0, \; \lambda_1 > 0$	$\mathbf{g} \cdot \mathbf{e}_1 = \mathbf{g} \cdot \mathbf{e}_2 = 0, \; \lambda_1, \lambda_2 > 0$

One way to inspect ridge surfaces (for example) in a volume is to densely sample $|\mathbf{g} \cdot \mathbf{e}_3|$ on a two-dimensional cutting plane and look for the dark lines indicating the ridge surface intersection with the plane. Figure 1 shows an example of FA ridge surfaces in a two-dimensional coronal slice of a human brain DTI scan[1]. For context, Figure 1(a) shows the standard RGB colormap of $\mathbf{e}_1$ at the original image resolution. Figures 1(b) and 1(c) illustrate how smooth features arise from convolution-based measurements of FA and ∇FA. Figure 1(d) uses contrast-enhancement to show the dark smooth lines indicating the ridge surfaces. The cubic spline used in this and all other results was 4mm between inflection points.

---

[1] DTI data was estimated from 30 DWIs at b $= 700\text{s/mm}^2$ and 5 non-DWI T2s, from a 1.5 T Philips scanner, with resolution $0.94 \times 0.94 \times 2.5\text{mm}$.

(a) RGB($\mathbf{e}_1$)   (b) FA   (c) $\mathbf{g} = |\nabla(\mathrm{FA})|$ (d) $|\mathbf{g} \cdot \mathbf{e}_3|^{1/3}$
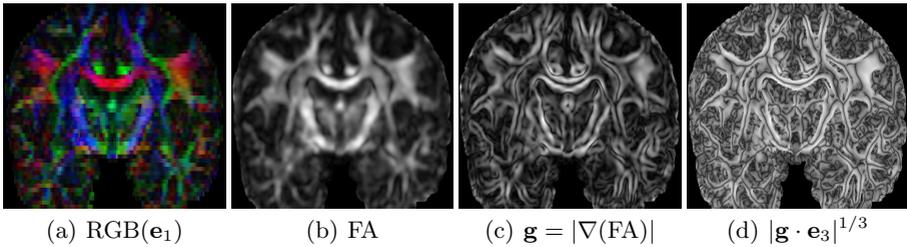
Fig. 1. Two-Dimensional Demonstration of Ridge Surface Evaluation

3.3   Crease Surface Extraction

We extract crease surfaces by per-voxel triangulation of the zero-isocontour of $\mathbf{g} \cdot \mathbf{e}_i$ ($\mathbf{g} \cdot \mathbf{e}_3$ for ridges, $\mathbf{g} \cdot \mathbf{e}_1$ for valleys) using Marching Cubes [17], taking care in evaluating $\mathbf{g} \cdot \mathbf{e}_i$ at voxel corners. Eigenvectors lack intrinsic sign, so $\mathbf{g} \cdot \mathbf{e}_i$ can suddenly change sign, far from a crease, simply due to the numerical properties of eigenvector computation. The literature offers ways to overcome this. Morse suggests determining correspondences between sets of eigenvectors rather than individual ones, to handle eigenvector permutations associated with eigenvalue equality [18]. Furst *et al.* use similar ideas in *Marching Cores* to extract crease manifolds in image scale-space [19]. For *Marching Ridges*, Furst and Pizer choose eigenvector signs to agree with the principal eigenvector of the average of outer products of the eigenvectors under consideration [20].

Our experience suggests that Hessian eigenvectors of non-linear scalar attributes of tensors (such as FA) tend to vary more rapidly than those of a similarly sampled scalar field. Accordingly, we explicitly determine eigenvector orientation consistency by traversing voxel edges to monitor eigenvector rotation. Samples are adaptively generated along voxel edges to satisfy an upper-bound on the angle between unsigned eigenvectors at successive samples. This determines whether the smooth transport of $\mathbf{e}_i(\mathbf{v}_0)$ from vertex $\mathbf{v}_0$ to vertex $\mathbf{v}_1$ agrees in sign with the eigenvector $\mathbf{e}_i(\mathbf{v}_1)$ computed at $\mathbf{v}_1$. The per-edge eigenvector sign information determines a per-voxel sign consistency prior to evaluating the Marching Cubes case. Inter-voxel sign inconsistencies lead to triangulations with inconsistent vertex windings. Thus, as a final pass, we traverse the surface mesh to fix vertex windings, which allows graphics hardware to appropriately render the crease surfaces with two-sided lighting [21].

The continuous tensor field measurements allow the voxel grid of the crease surface triangulation to be independent of the underlying data resolution. The results in Section 4 use a triangulation resolution two to three times that of the data. The strength of the crease surface is assessed with the appropriate Hessian eigenvalue ($-\lambda_3$ for ridges, λ_1 for valleys) so that geometry is extracted only for significant features.

4   Results

Figure 2 shows ridge detection results on the same cutting plane used in Figure 1. Ridge strength is mapped in Figure 2(a), the coherent organization of which is

(a) $\max(-\lambda_3, 0)$ (b) Ridge surfaces   (c) $((\mathbf{g} \cdot \mathbf{e}_2)^2 + (\mathbf{g} \cdot \mathbf{e}_3)^2)^{1/6}$
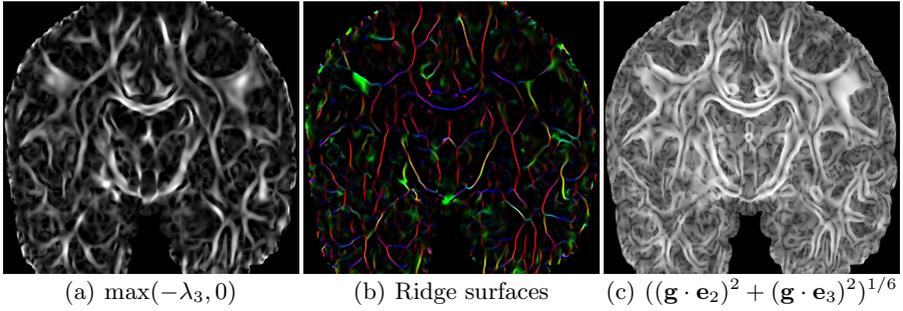
Fig. 2. Two-Dimensional Ridge Surface and Ridge Line Results

(a) RGB Map with Fibers   (b) Ridge Surfaces

(c) Valley Surfaces   (d) Valleys with Fibers
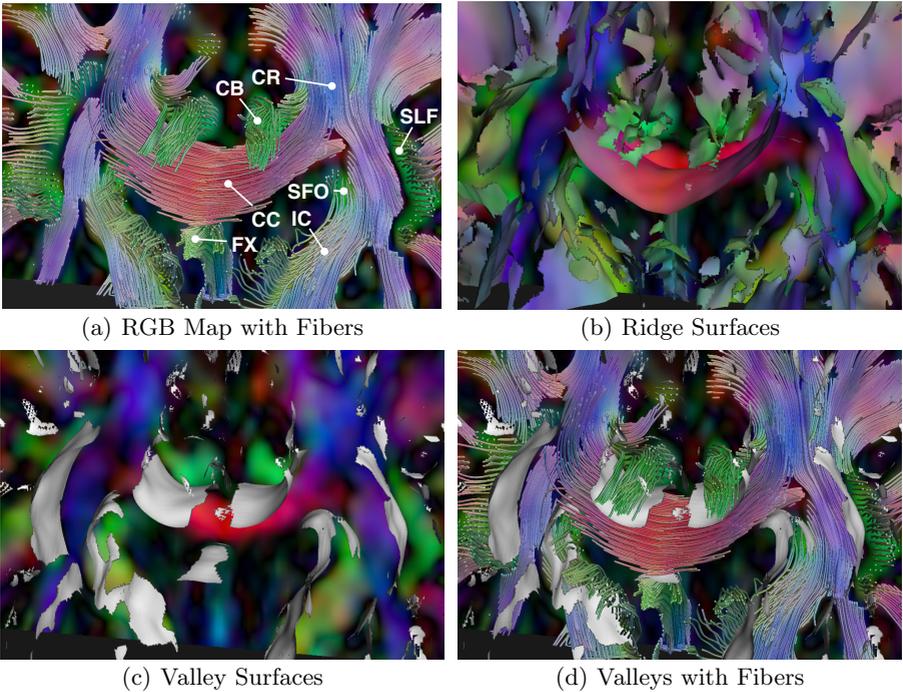
Fig. 3. Anisotropy Creases Near the Corpus Callosum

suggestive of white matter pathways. A combination of ridge strength masking, contrast enhancement, and RGB directional encoding created Figure 2(b) from Figure 1(d), to highlight the lines through major white matter pathways. Figure 2(c) maps a quantity that is zero on ridge *lines* of FA, intersecting the plane in points. Multiple lines lie within the corpus callosum, but there are two clear dots within the cingulum bundles, and one in the fornix, consistent with the shape and orientation of these tracts relative to this coronal plane.

The renderings in Figure 3 (from a posterior viewpoint) show a cropped region around the same coronal slice of previous figures. In Figure 3(a) fibers are seeded

(a) RGB Map with Fibers

(b) Ridge Surfaces

(c) Valley Surfaces

(d) Ridges and Valleys with Fibers
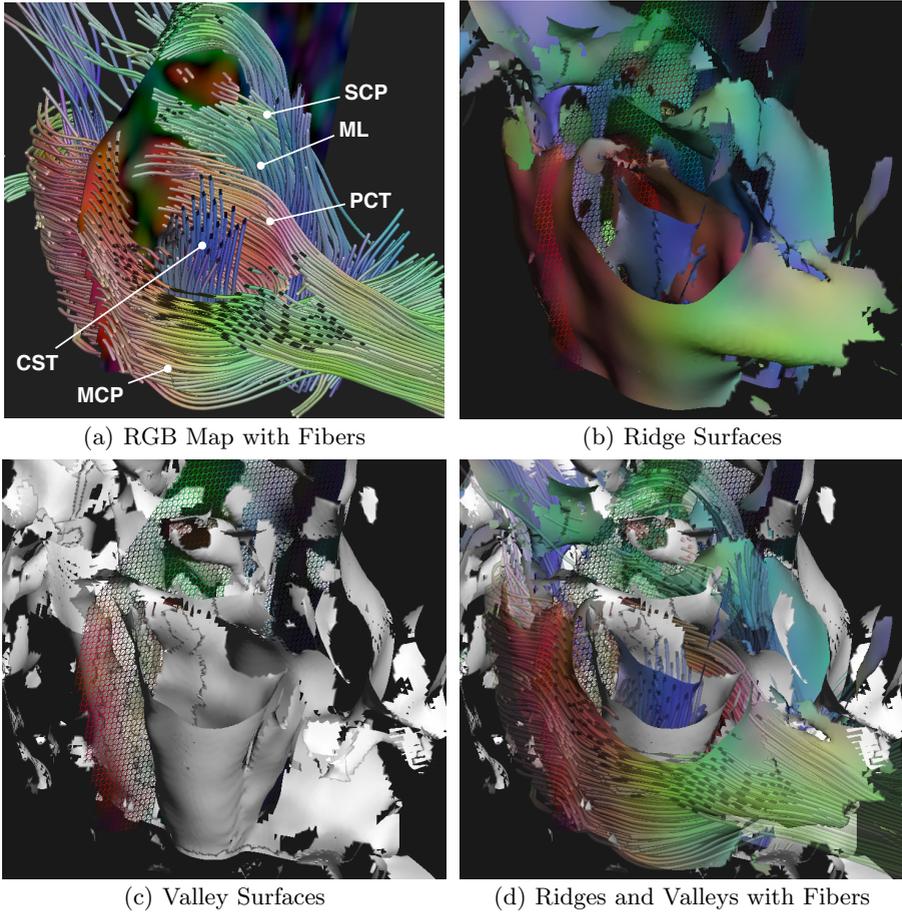
Fig. 4. Anisotropy Creases in the Brainstem

from the RGB encoded plane. Figure 3(b) shows how the ridge surfaces (using the same RGB encoding) follow major fiber paths, especially the corpus callosum (CC), internal capsule (IC), corona radiata (CR), and fornix (FX) [22]. The (white) anisotropy valley surfaces in Figure 3(c) delineate interfaces between the CC and cingulum bundles (CB), superior fronto-occipital fasciculus (SFO) and IC, and IC and superior longitudinal fasciculus (SLF). Figure 3(d) also illustrates how anisotropy valleys lie between adjacent paths of differing orientation.

Figure 4 illustrates anisotropy crease analysis in the brainstem (lateral anterior superior viewpoint), starting with (in Figure 4(a)) a plane seeding fibers for anatomical context. Here, a viewpoint-aligned cutting plane partially cuts into the middle cerebellar peduncle (MCP) to reveal the corticospinal tract (CST) and pontine crossing tract (PCT), anterior to the medial lemniscus (ML) and superior cerebellar peduncle (SCP). These pathways appear as distinct anisotropy ridge surfaces in Figure 4(b), and their interfaces are delineated by the valley

surfaces in Figure 4(c), especially the enclosure of CST between MCP and PCT. Figure 4(d) combines the crease surfaces with faint fibers to illustrate how the alternating layers of ridges and creases combine to form a fiber path skeleton.

5   Discussion and Future Work

Anisotropy creases model white matter structure from DTI using continuously measured anisotropy derivatives and explicitly triangulated surface geometry. The invariance properties of their mathematical definition help give anisotropy creases the attractive property of being parameter free (aside from the choice of convolution kernels), in contrast to most tractography and clustering algorithms.

Future work will include extraction of FA ridge *lines*, and their comparison to individual fiber tracts. An interesting question left unanswered is why strong valley surfaces of FA reliably indicate adjacent orthogonal tracts, considering that FA is simply a scalar invariant, with no knowledge of nearby eigenvectors. Finally, to extract true image *cores*, crease detection must work across measurement scales [19], which we have not yet implemented. Prior anatomical knowledge may usefully constrain, however, the necessary scale range. For example, extracting fiber interfaces as anisotropy valleys may require only a single image scale, considering that the interfaces are not apt to have much physical thickness, thus the measurement scale is determined by the acquisition resolution.

We hope to use anisotropy creases with non-rigid tensor registration, first analyzing existing methods according to how well anisotropy creases are aligned, and then perhaps enhancing registration to use the creases as fiducials.

Acknowledgements

References

1. Basser, P., Jones, D.: Diffusion-tensor MRI: Theory, experimental design and data analysis - A technical review. Nuc Mag Res in Biomed **15** (2002) 456–467
2. Mori, S., Zijl, P.V.: Fiber tracking: Principles and strategies - A technical review. Nuc Mag Res in Biomed **15** (2002) 468–480
3. Corouge, I., Fletcher, P., Joshi, S., Gilmore, J., Gerig, G.: Fiber tract-oriented statistics for quantitative diffusion tensor MRI analysis. In: Eighth International Conference on Medical Image Computing and Computer-Assisted Intervention (MICCAI'05). (2005) 131–139
4. Moberts, B., Vilanova, A., van Wijk, J.: Evaluation of fiber clustering methods for diffusion tensor imaging. In: Proceedings of IEEE Visualization 2005. (2005) 65–72

5. Basser, P.: Inferring microstructural features and the physiological state of tissues from diffusion-weighted images. Nuc Mag Res in Biomed **8** (1995) 333–344
6. Kubicki, M., Westin, C.F., Maier, S., Mamata, H., Frumin, M., Ernst-Hirshefeld, H., Kikinis, R., Jolesz, F., McCarley, R., Shenton, M.: Cingulate fasciculus integrity disruption in schizophrenia: A magnetic resonance diffusion tensor imaging study. Biological Psychiatry **54** (2003) 1171–1180
7. Eberly, D., Gardner, R., Morse, B., Pizer, S.: Ridges for image analysis. Journal of Mathematical Imaging and Vision **4** (1994) 351–371
8. Smith, S., Jenkinson, M., Johansen-Berg, H., Rueckert, D., Nichols, T., Mackay, C., Watkins, K., Ciccarelli, O., Cader, M., Matthews, P., Behrens, T.: Tract-based spatial statistics: Voxelwise analysis of multiple-subject diffusion data. Technical Report TR05SS1, Oxford University Centre for Functional MRI of the Brain (2006)
9. de Saint-Venant, M.: Surfaces à plus grande pente constituées sur des lignes courbes. Bulletin de la Société Philomathématique de Paris (1852) 24–30
10. Haralick, R.M.: Ridges and valleys on digital images. Computer Vision, Graphics, and Image Processing **22** (1983) 28–38
11. Maxwell, J.: On hills and dales. The London, Edinburgh and Dublin Philosophical Magazine and Journal of Science **40**(269) (1870) 421–425
12. Gauch, J.M., Pizer, S.M.: Multiresolution analysis of ridges and valleys in grey-scale images. IEEE Trans Pat Analysis and Mach Int **15**(6) (1993) 635–646
13. Pajevic, S., Aldroubi, A., Basser, P.: A continuous tensor field approximation of discrete DT-MRI data for extracting microstructural and architectural features of tissue. Journal of Magnetic Resonance **154** (2002) 85–100
14. O'Donnell, L., Grimson, W., Westin, C.F.: Interface detection in diffusion tensor MRI. In: Seventh International Conference on Medical Image Computing and Computer-Assisted Intervention (MICCAI'04). (2004) 360–367
15. Aldroubi, A., Basser, P.: Reconstruction of vector and tensor fields from sampled discrete data. Contemporary Mathematics **247** (1999) 1–15
16. Gonzalez, R., Woods, R.: Digital Image Processing. 2nd edn. Addison-Wesley Publishing Company, Reading, MA (2002)
17. Lorensen, W.E., Cline, H.E.: Marching cubes: A high resolution 3D surface construction algorithm. Computer Graphics **21**(4) (1987) 163–169
18. Morse, B.S.: Computation of Object Cores from Grey-Level Images. PhD thesis, University of North Carolina at Chapel Hill, Chapel Hill, NC (1994)
19. Furst, J.D., Pizer, S.M., Eberly, D.H.: Marching cores: A method for extracting cores from 3d medical images. In: Proceedings of IEEE Workshop on Mathematical Methods in Biomedical Image Analysis. (1996) 124–130
20. Furst, J.D., Pizer, S.M.: Marching ridges. In: Proceedings of 2001 IASTED International Conference on Signal and Image Processing. (2001)
21. Shreiner, D., Woo, M., Neider, J., Davis, T.: OpenGL Programming Guide. Fourth edn. Addison-Wesley (2004)
22. Mori, S., Wakana, S., Nagae-Poetscher, L., Zijl, P.V.: MRI Atlas of Human White Matter. Elsevier (2005)